Engineering protein nanoparticles out from components of the human microbiome

Hèctor López-Laguna, Laura Sánchez-García, Naroa Serna, Eric Voltà-Durán, Julieta M. Sánchez, Alejandro Sánchez-Chardi, Ugutz Unzueta*, Marcin Los, Antonio Villaverde* and Esther Vázquez

Hèctor López-Laguna, Dr. Laura Sánchez-García, Dr. Naroa Serna, Eric Voltà-Durán, Dr. Julieta M. Sánchez, Dr. Antonio Villaverde, Dr. Esther Vázquez
Institut de Biotecnologia i de Biomedicina, Universitat Autònoma de Barcelona, Bellaterra, 08193 Barcelona, Spain

Hèctor López-Laguna, Dr. Laura Sánchez-García, Dr. Naroa Serna, Eric Voltà-Durán, Dr. Julieta M. Sánchez, Dr.Ugutz Unzueta, Dr. Antonio Villaverde, Dr. Esther Vázquez
Departament de Genètica i de Microbiologia, Universitat Autònoma de Barcelona, Bellaterra, 08193 Barcelona, Spain

Hèctor López-Laguna, Dr. Laura Sánchez-García, Dr. Naroa Serna, Eric Voltà-Durán, Dr. Julieta M. Sánchez, Dr. Ugutz Unzueta, Dr. Antonio Villaverde, Dr. Esther Vázquez
CIBER de Bioingeniería, Biomateriales y Nanomedicina (CIBER-BBN), C/ Monforte de Lemos 3-5, 28029 Madrid, Spain

Dr. Julieta M. Sánchez Instituto de Investigaciones Biológicas y Tecnológicas (IIBYT) (CONICET-Universidad Nacional de Córdoba), ICTA & Cátedra de Química Biológica, Departamento de Química, FCEFyN, UNC. Av. Velez Sarsfield 1611, X 5016GCA Córdoba, Argentina

Dr. Alejandro Sánchez-Chardi Servei de Microscòpia, Universitat Autònoma de Barcelona, Bellaterra, 08193 Barcelona, Spain

Dr. Alejandro Sánchez-Chardi Departament de Biologia Evolutiva, Ecologia i Ciències Ambientals, Facultat de Biologia, Universitat de Barcelona, Av. Diagonal 643, 08028 Barcelona, Spain

Dr.Ugutz Unzueta Institut d'Investigacions Biomèdiques Sant Pau and Josep Carreras Research Institute, Hospital de la Santa Creu i Sant Pau, 08041 Barcelona, Spain

Dr. Marcin Los Department of Bacterial Molecular Genetics, Faculty of Biology, University of Gdansk, Wita Stwosza Street 59, 80-308 Gdansk, Poland

Dr. Marcin Los Phage Consultants, Partyzantow Street 10/18, 80-254 Gdansk, Poland

E-mail: uunzueta@santpau.cat; antoni.villaverde@uab.es

Abstract

Nanoscale protein materials are highly convenient as vehicles for targeted drug delivery because of their structural and functional versatility. Selective binding to specific cell surface receptors and penetration into target cells require the use of targeting peptides. Such homing stretches should be incorporated to larger proteins that do not interact with body components, to prevent undesired drug release into non-target organs. Because of their low interactivity with human body components and their tolerated immunogenicity, proteins derived from the human microbiome are appealing and fully biocompatible building blocks for the biofabrication of non-reactive, inert protein materials within the nanoscale. Several phage and phage-like bacterial proteins with natural structural roles have been produced in *Escherichia coli* as polyhistidine-tagged recombinant proteins, looking for their organization as discrete, nanoscale particulate materials. While all of them self-assembled in a variety of sizes, the stability of the resulting constructs at 37 ℃ was found to be severely compromised. However, the fine adjustment of temperature and Zn^{2+} concentration allowed the formation of robust nanomaterials, fully stable in complex media and under physiological conditions. Then, microbiome-derived proteins show promises for the regulatable construction of scaffold protein nanomaterials, which can be tailored and strengthened by simple physicochemical approaches.

Protein materials are gaining interest in nanomedicine as drug carriers [1-3] since they offer full biocompatibility and biodegradability. In addition, proteins and derived constructs are structurally and functionally versatile. Their feasible production at industrial scale by well-established recombinant DNA procedures allows their widespread clinical use. [4] In this context, hydrogels, fibers, layers but especially nanoparticles are engineered as drug-releasing systems or as carriers of drugs or imaging agents for cell-targeted delivery. Targeting can be reached by functionalization with peptidic ligands of cell surface markers [5] that allow selective cell binding and internalization. Precision drug delivery is specially needed in cancer therapies in which most of the used drugs are highly cytotoxic. [6, 7] The nanoscale size of the resulting protein-drug conjugates would prevent renal filtration of the payload, usually small molecular weight chemicals, but it also favors the enhanced permeability and retention effect (EPR) in tumor tissues. [8] Among the few examples of protein-drug nanoscale complexes approved for use, Abraxane® (Nab-Paclitaxel) is indicated for breast, lung and pancreas cancers. [9] In this formulation, the drug Paclitaxel is stabilized by human albumin [10] that in form of clusters of around 130 nm confers the desired nanoscale size although not receptor-mediated cancer cell targeting. [11] The albumin in such complexes is a convenient drug carrier because of its human nature and the expected absence of intrinsic immunogenicity associated to repeated administration. However, because of its multiple organic roles, human albumin is highly interactive with a large catalogue of molecules, cells and tissues of the human body. [12] This fact prevents the optimal tumor biodistribution of the drug because of the wide spectrum of multiple binding targets of the complex. The use of highly reactive human proteins would be then an obstacle for selective cell targeting even when functionalized with appropriate target cell surface ligands, that might unable to overcome the intrinsic interactivity of the carrier protein. Ideally, for a proper utilization in clinics, protein materials aimed to assist in

drug delivery (but also in other medical applications such as when used as scaffolds in tissue engineering) should be non-immunogenic, as in the case of human albumin, but also non-reactive. At some extent, these are not matching properties since human proteins, being non-immunogenic, have evolved to perform multiple interactions. On the other hand, non-human proteins, lacking strong interactions with components of the human body, should not alter the selectivity conferred by homing peptides (as recently shown with GFP-based constructs [13]), but they might potentially elicit undesired immune responses.

For a proper selection of building blocks for protein materials, a compromise between lack of reactivity and low immunogenicity can be found in the proteome of the non-pathogenic fraction of the human microbiome. In this regard, bacterial cells and their bacteriophages, being usual symbionts of the human body, are especially appealing. In the case of phages, the rising of bacterial strains with multi-resistance to antibiotics has even promoted to reconsider them as promising bacteria killing agents, [14] assuming a moderate immunogenicity acceptable at the regulatory level. [15, 16] This assumption, as well as the related set of evidences in this direction supported the entry of several bacteriophage species into clinical trials, for both local and systemic applications, as antimicrobial drugs [17] (see in addition both the ongoing and already completed clinical trials NCT02116010, NCT01818206 and NCT03140085 at https://clinicaltrials.gov/).

Sustained by this concept, we selected several phage and bacterial proteins from the human microbiome (Figure 1A), with presumed ability to self-assemble because of their structural roles in the original microorganisms. These proteins were tagged with a hexahistidine tail (H6) for affinity purification from bacterial cell extracts and screened for their ability to self-assemble as nanostructures that should be stable under physiological conditions (namely moderated ionic strength, physiological pH and 37 ºC). The selected polypeptides were the *Pseudomonas aeruginosa* HCP1 protein, an element of the type VI secretion system structurally related to the tail protein of phage lambda, [18] the major phage lambda capsid D

protein (abbreviated here as PLD, [19]) and P3, a major capsid protein of phage PRD1

(abbreviated here as MCP3, [20]) that infects enterobacteria and that is also a component of the

human microbiome [21] (Figure 1A). In their natural sources, all these proteins are found

assembled, together with other protein partners, as rod-like structures (HCP1 and PLD

proteins) or as members of icosahedral, adenovirus-like protein complexes (MCP3). HCP1-

H6, MCP3-H6 and PLD-H6 were all produced in *Escherichia coli* and purified from cell

extracts as proteolytically stable full-length fusions (Figure 1B). At this point, we wondered if

these proteins, out of their natural context, would still keep their self-organizing properties. At

exception of PLD-H6, whose hydrodynamic diameter was compatible with the unassembled

monomeric form (< 4 nm), the other two proteins spontaneously organized as supramolecular

structures with sizes above the renal cut-off, estimated to be around 6-8 nm. [22] HCP1-H6

self-assembled as entities over 8 nm in diameter (Figure 1C,D), compatible with hexameric

forms (Figure 1E) in which the protein has been naturally described. [23] On the other hand,

MCP3-H6 assembled as structures of 23 nm (Figure 1C,D), over the size of the natural

oligomers (Figure 1E). No differences in bacterial DNA content were observed, that might

have accounted for a differential propensity to form protein complexes. Z potential was

negative in all cases (Figure 1D) and far from aggregation-prone values. The molecular

masses determined by MALDI-TOF were also congruent with the electrophoretic mobility of

the proteins (Figure 1B, D). As a reference of the molecular size, 3D models of monomers and

the natural oligomeric forms of these proteins are shown in Figure 1E.

When screening parameters potentially involved in the formation of supramolecular protein

complexes, and therefore, useful to control the oligomerization process, temperature was

considered as an important modulator. [24] Importantly, any protein complex should be stable

at the body temperature as a necessary condition for its potential clinical use. The

nanoparticles formed by HCP1-H6 were stable at 37ºC and distinguishable from microscale

aggregates occurring at higher temperatures (Figure 2A). In contrast, MCP3-H6 nanoparticles

aggregated already at 37ºC, while at this temperature PLD-H6 remained unassembled but nanoparticles were formed at 50ºC (Figure 2A). To check the temperature dependence of PLD-H6 assembly, this protein was incubated at progressively growing temperatures and the size of the resulting materials were checked in each step. As observed (Figure 2B), oligomerization of this protein started around 40 ºC and the nanoparticles remained assembled under further heating but also when cooling back to 10 ºC (Figure 2B). This was indicative of an irreversible assembly process, that boosted by temperature rendered supramolecular materials stable at physiological conditions. In this context, the CD analysis of PLD-H6 (Supplementary Figure 1) revealed a more stable alpha helix structure upon heating, as the two alpha helix minima became then evident (one noticeable minimum at 208 nm and an incipient one at 220 nm) simultaneous to the nanoparticle formation. The formation of these nanoparticles was observed in a wide range of protein concentrations, namely between 0.05 mg/mL and 11 mg/mL (not shown), proving to be an event different from plain protein aggregation that is highly dependent on protein concentration.

On the other hand, and to test if the aggregation of MCP3-H6 at 37ºC could be prevented, we added Zn^{2+} to protein samples. Generically, divalent ions are stabilizers of protein-protein interactions mediated by histidine residues, and this principle has been recently used for the in vitro generation of protein clusters at the micro scale, using hexahistidine-tagged proteins as building blocks. [25] Indeed, physiological amounts of Zn^{2+} were able to prevent temperature-mediated aggregation of MCP3-H6 (Figure 2C), rendering stable nanoparticles of around 45 nm at 37 ºC. Aggregation was then only observed at around 50 ºC, far from the clinically relevant temperature range. Interestingly, Zn^{2+} had a stabilizing effect over the three tested proteins (Figure 2E), proving the effectiveness of divalent ions in regulating protein-protein contacts. The proper selection of Zn^{2+} concentrations, always within physiological values, permitted not only preventing aggregation but also tuning the size of the supramolecular complexes (Figure 2E). At high doses, the metal promoted the collapse of PLD-H6 into

aggregates (Figure 2E), probably by enhancing cross-molecular contacts above those supporting a regular supramolecular organization, in agreement with previous data. [26] Also, the optimal size range for drug delivery (between 20 and 80 nm, depending on the experimental settings) was maintained in the resulting nanoparticles, even under increasing temperatures as observed for HCP1-H6 (Figure 2D). [1, 7, 27] It must be noted that PLD-H6 was less responsive than the alternative constructs to size tuning.

On the other side, Zn^{2+} promoted protein oligomerization through conformational changes in the whole protein nanoparticles ($CSM_{+ZnCl2} \neq CSM_{-ZnCl2}$) (Figure 2F). Such conformational modifications were remarkable in HCP1-H6 but almost negligible for MCP3-H6, which showed the highest stability (CSM values almost unchanged). The modest increase in the CSM values of HCP1-H6 and PLD-H6 versus temperature (up to 45ºC) suggested a notable stability (Figure 2F). The presence of Zn^{2+} did not affect the whole thermal profile of any of the protein complexes (Figure 2F, insets), and the Z potential was not modified during oligomerization (Figure 2G).

A summary of optimal temperature and Zn^{2+} concentrations for the nanoscale organization of these three proteins is presented in Figure 3A. Interestingly, the stabilized HCP1-H6 and MCP3-H6 proteins rendered regular, discrete nanoparticles with a toroid disposition (Figure 3A, B) and compatible with their natural oligomeric forms (Figure 1E). Note that PLD-H6 generated, instead, short fibril-like structures (Figure 3B). Since amphiphilicity was not particularly evident in any of the involved proteins, their assembly would be not linked to such property (Supplementary Figure 2). In addition, the materials did not disassemble when incubated at 37 ºC in complex cell media, neither in consecutive freezing or thawing conditions (Figure 3C), although a slight increase in the hydrodynamic size was observed. Interestingly, imidazole, known to softly disrupt histidine-based cross-interactions, [28] was also unable to disassemble the nanoparticles, and EDTA, known as a strong divalent cation chelating agent, [29] only compromised the stability of HCP1-H6 oligomers (Figure 3D).

Altogether, these data indicated that Zn^{2+} contributed to the formation of the oligomers and at least partially, to their stability (Figure 2 and 3) in form of a cross-linking agent.

Protein assemblies at the nanoscale, acting as mimetics of viral capsids, are of emerging interest in nanomedicine as drug delivery systems and for applications in theragnostics because of the easy manipulability, functionality and intrinsic biocompatibility of such macromolecules. [30] However, for systemic uses, limited immunogenicity and specially poor or null reactivity with human body components are desired. Such combination of parameters cannot accomplished by human proteins, which while devoid of immunogenicity are highly interactive with multiple ligands in the body. Components of the non-pathogenic human microbiome are particularly appealing since they are in close contact with human populations and expected to be well produced in recombinant versions as assembly-prone materials. Although whole phages or phage-derived virus-like particles have been already tested as drug carriers, [31] the differential immunogenicity exhibited by individual phage proteins [16] strongly pushes towards the construction of materials based on single selected protein species. In this context, we have tested here three microbial structural proteins with potential for self-assembling (Figure 1). We have also demonstrated how the precise but simple control of temperature and Zn^{2+} ion concentration (Figure 2) is sufficient to promote the formation of robust nanoscale structures at a wide range of protein concentrations, fully stable at the body temperature and in complex media (Figure 3) and completely different from plain protein aggregates that show microscale dimensions (Figure 2). Interestingly, Zn^{2+} is involved in the formation of robust supramolecular constructs (Figures 2C, 2D, 2E, 3A and 3D) in a concentration-dependent way (Figure 2E). Such architectonic role is specifically relevant in the case of HCP1-H6, as the oligomers formed by this construct were disassembled by EDTA through Zn^{2+} removal (Figure 3D). This can be due to the metal coordination regulating the positioning of the building blocks in the oligomers through cross-interactions with the H6 tails of HCP1-H6. Then, the metal itself appears to be an important architectonic agent.

Interestingly, Zn^{2+} is also observed as a stabilizer of the materials since it prevented aggregation of MCP3-H6 at 37 ºC (Figure 2C). Interestingly, in the case of PLD-H6 and irrespective of the role of Zn^{2+} (Figure 2E), the formation of stable nanoparticles is achieved through an energy influx in form of heat.

Conclusion

In summary, we propose here a new conceptual approach to generate biologically inert protein scaffold materials in the nanoscale, with potential for clinical applications. This concept is based on the use of protein components of the human microbiome with poor or null reactivity with human cells and tissues, that once assembled might serve as nanoscale drug vehicles for cell-targeted drug delivery. Such strategy benefits from the huge catalogue of structural proteins abounding in the phage fraction of the microbiome, which is progressively identified. The three proteins selected here are just a representative sample of such spectrum of potential building blocks, but they illustrate how the natural tendency to form nanostructures can be modulated, out of their natural context, by simple physicochemical methods. Among the strategies to generate protein nanoscale materials,[1, 2, 32] the microbiome-based approach is of special interest because the construction of supramolecular complexes based on structural microbial proteins does not require a fully *de novo* architectonic design but instead, it is supported by their oligomerization-prone nature.

Experimental Section

Protein genetic design, production and purification

All protein sequences were designed as codon-optimized genes and cloned into pET22b by using NdeI and HindIII restriction enzymes. The recombinant plasmids were provided by GeneArt (ThermoFisher) and transformed into *Escherichia coli* Origami B (BL21, OmpT−, Lon−, TrxB, Gor−; Novagen) by heat shock at 42 ºC for 45 sec. All encoded proteins were produced overnight at 20 ºC at 250 rpm agitation, upon addition of 0.1 mM isopropyl-β-d-thiogalactopyronaside (IPTG) when the OD_{550} reached 0.5-0.7. Cells were harvested by centrifugation at 5,000 g, at 4 ºC for 15 min and stored at -80 ºC. For protein recovery, pellets were thawed and resuspended in wash buffer (20 mM Tris HCl, 500 mM NaCl, 10 mM Imidazole, pH = 8.0) in presence of protease inhibitors (complete EDTA-free; Roche Diagnostics). Cell disruption was achieved in two rounds in a French Press (Thermo FA-078) at 1,200 psi. The soluble fraction was then separated by centrifugation at 4 ºC, 15,000 *g* for 45 min and the supernatant consecutively filtered through 0.45 and 0.22 µm pore filters. Proteins were purified by Immobilized Metal Affinity Chromatography (IMAC) in an ÄKTA pure system (GE Healthcare) using 5 mL HisTrap columns (GE Healthcare). Protein elution was achieved by a linear gradient of Elution buffer (20 mM Tris HCl, 500 mM NaCl, 500 mM Imidazole, pH = 8.0) and the rinsed protein was dialyzed against both sodium carbonate (166 mM $NaCO_3H$, pH = 8.0) or sodium carbonate with salt (166 mM $NaCO_3H$ + 333 mM NaCl, pH = 8.0) buffers.

Protein purity, concentration and integrity

Protein purity was assessed by using a 12 % TGX Stain-Free ™ FastCast™ Acrylamide Kit (BioRad). After electrophoresis, protein bands were subsequently transferred by Trans-Blot® Turbo™ Transfer System (BioRad) into PVDF membranes and immunodetected with an anti-

His (Santa Cruz Biotechnology) monoclonal antibody. Protein concentration was determined by Bradford's assay and their integrity checked by Matrix-assisted Laser Desorption Ionization Time-of-Flight (MALDI-TOF) mass spectrometry.

Volume size distribution, surface charge and ultrastructural morphometry

The hydrodynamic diameter of proteins was determined by Dynamic Light Scattering (DLS), and protein surface charge, expressed as Z-potential (Zp) in mV, by Electrophoretic Light Scattering (ELS), both at 633 nm, in a Zetasizer Nano ZS using ZEN2112 3 mm quartz batch cuvettes and DTS10170 capillary cells, respectively, at 25 °C. The Polydispersion Index (PDI) was determined for all samples. Field emission scanning electron microscopy (FESEM) [13] and transmission electron microscopy (TEM) imaging of protein samples was performed using a conventional negative staining technique as previously described. [33]

DNAbc content

Bicatenary DNA content (DNAbc) was determined from the absorbance ratio between 260 and 280 nm (A_{260}/A_{280}). All measurements were performed in a Nanodrop One System (ThermoFisher).

Oligomerization status onto thermal kinetics

Protein size was analyzed at increasing temperatures (namely 4, 10, 20, 30, 37 and 50 °C) by DLS. Protein concentration was initially adjusted at 2 mg/mL in all cases.

Zinc-mediated protein assembling

Proteins were exposed to increasing concentrations of $ZnCl_2$ depending on their aggregation or oligomerization tendencies. The size of the resulting materials was subsequently analyzed by DLS and data expressed in nm. Protein concentration was initially tested up to 11 mg/mL

and finally adjusted at 2 mg/mL in all cases, for a convenient manipulation of ion

concentrations at physiological values.

Intrinsic fluorescence versus temperature

Fluorescence spectra were recorded in a Cary Eclipse spectrofluorimeter (Agilent

Technologies), using a quartz cell with 10 mm path length and a thermostated holder. The

excitation and emission slits were set at 5 nm. Excitation wavelength (λ_{ex}) was set at 295 nm.

Emission spectra were acquired between 310 and 450 nm in protein samples at 0.2 mg/mL,

dissolved in sodium carbonate buffer with salt. The temperature-dependent behavior of

proteins was determined between 25 and 85 ℃ in p/a of $ZnCl_2$ (0.196 mM). The Centre of

Spectral Mass (CSM), a weighted average of the fluorescence spectrum peaks, was calculated

[34] for comparison. The CSM is also related with the relative exposure of the tryptophan (Trp)

to the protein environment. The maximum red-shift in the CSM of Trp is compatible with

large solvent accessibility. [35]

Thermal and chemical stability

Proteins, in their oligomerized form, were exposed to different temperatures (room

temperature, 37 ℃ and freezing/thawing cycles at -80 ℃) and chemical compounds (NaCl,

EDTA, imidazole at 0.2 mM final concentration and OptiPro complex cell culture media).

The size of protein constructs was subsequently analyzed by DLS and data expressed in nm.

Protein concentration was initially adjusted at 2 mg/mL in all cases.

Circular dichroism

Far-UV circular dichroism (CD) was measured at 25℃ in a Jasco J-715 spectropolarimeter to

assess secondary structure. Protein concentration was adjusted to 0.2 mg/mL in 166 mM

carbonate-bicarbonate, at pH 8. The CD spectra were obtained with a 0.2 mm pathlength

cuvette over a wavelength range of 190-240 nm. The scan rate was 100 nm/min with a

response of 2 s and a bandwidth of 1 nm, and a total of 13 scans were accumulated. The

spectra were processed through a negative exponential fit with a sampling proportion of 0.1

and 1 polynomial degree.

In silico calculations

UCSF Chimera software was used for *in silico* representation, structural hydropathicity

pattern visualization and theoretical measurement of distances (nm) in X-ray 3D diffraction

structures of proteins. The data set was extracted from the Protein Data Bank Database (PDB)

and the corresponding codes were 1Y12 for HCP1, 1CJD for MCP3 and 1C5E for PLD. The

resulting analysis illustrates the sterical and physicochemical nature of protein building

blocks.

Statistical analysis

Quantitative data were expressed as mean ($\overline{x}$) ± Standard Error of the Mean (SEM) and all

measurements were performed at least in triplicate (n = 3). In all cases, an initial normality

and lognormality analyses were performed including Anderson-Darling, D'Agostino &

Pearson, Shapiro-Wilk and Kolmogorov-Smirnov tests to determine the normal distribution

(behavior). The parametric data were analyzed by one or two-ways ANOVA or *t*-tests

depending on the number of groups and conditions. The nonparametric data were analyzed by

Kruskal-Wallis tests. All comparisons were performed in relation to either the control group

or the initial temperature (*$p < 0.05$).

Supporting Information

Supporting Information is available from the Wiley Online Library or from the author.
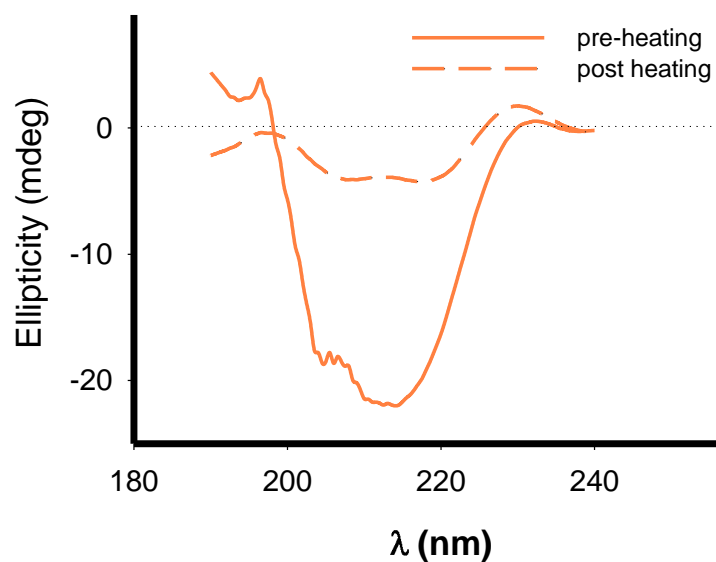
Supplementary Figure 1. Far UV CD of PLD-H6 before and after heating the protein sample at 45 ºC for 10 minutes.
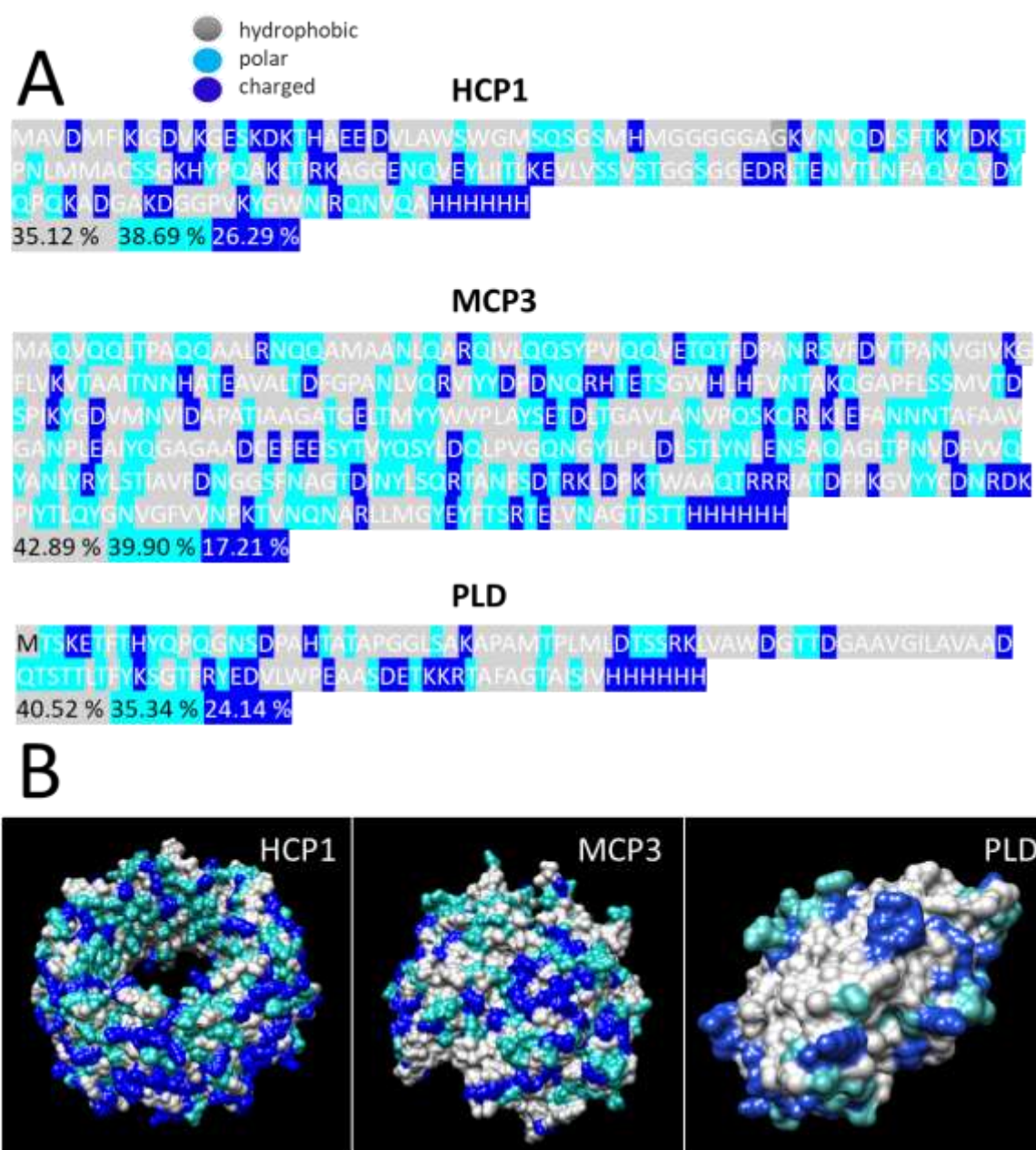
Supplementary Figure 2. Hydropathicity pattern of protein building blocks over the amino acid sequence (A) and structure (B) of the assembled proteins used in this study (see Figure 1E). None of them presents an unambiguous amphiphilic disposition, as polar and charged residues do not show a biased distribution over their surfaces.

References

[1]   D. Verma, N. Gulati, S. Kaul, S. Mukherjee, U. Nagaich, Journal of pharmaceutics **2018**, 9285854.

[2]   H. M. G. Sutherland T.D. Rapson T.D., Church J.S., in *Fibrous Proteins: Structures and Mechanisms.*, Vol. 82 (Ed: S. J. Parry D.), Springer, Cham **2017**.

[3]   G. Wei, Z. Su, N. P. Reynolds, P. Arosio, I. W. Hamley, E. Gazit, R. Mezzenga, Chemical Society reviews **2017**, 46, 4661; M. Abbas, Q. Zou, S. Li, X. Yan, Advanced materials **2017**, 29; Z. Wang, K. Zhi, Z. Ding, Y. Sun, S. Li, M. Li, K. Pu, J. Zou, Seminars in cancer biology **2020**; I. Casanova, U. Unzueta, I. Arroyo-Solera, M. V. Cespedes, A. Villaverde, R. Mangues, E. Vazquez, Current opinion in pharmacology **2019**, 47, 1.

[4]   L. Sanchez-Garcia, L. Martin, R. Mangues, N. Ferrer-Miralles, E. Vazquez, A. Villaverde, Microbial cell factories **2016**, 15, 33.

[5]   E. Vazquez, R. Mangues, A. Villaverde, Nanomedicine **2016**, 11, 1333.

[6]   K. Ozturk-Atar, H. Eroglu, S. Calis, Journal of drug targeting **2018**, 26, 633.

[7]   S. Raj, S. Khurana, R. Choudhari, K. K. Kesari, M. A. Kamal, N. Garg, J. Ruokolainen, B. C. Das, D. Kumar, Seminars in cancer biology **2019**.

[8]   D. Kalyane, N. Raval, R. Maheshwari, V. Tambe, K. Kalia, R. K. Tekade, Materials science & engineering. C, Materials for biological applications **2019**, 98, 1252; M. S. Lee, E. C. Dees, A. Z. Wang, Oncology **2017**, 31, 198; A. Nel, E. Ruoslahti, H. Meng, ACS nano **2017**, 11, 9567.

[9]   A. M. Sofias, M. Dunne, G. Storm, C. Allen, Advanced drug delivery reviews 2017; W. J. Gradishar, Expert opinion on pharmacotherapy **2006**, 7, 1041.

[10]   M. R. Green, G. M. Manikhas, S. Orlov, B. Afanasyev, A. M. Makhson, P. Bhar, M. J. Hawkins, Ann Oncol **2006**, 17, 1263.

[11]   B. Bhushan, V. Khanadeev, B. Khlebtsov, N. Khlebtsov, P. Gopinath, Advances in colloid and interface science **2017**, 246, 13.

[12]   K. W. Lexa, E. Dolghih, M. P. Jacobson, PloS one **2014**, 9, e93323; V. Arroyo, R. Garcia-Martinez, X. Salvatella, Journal of hepatology **2014**, 61, 396; M. Taverna, A. L. Marie, J. P. Mira, B. Guidet, Annals of intensive care **2013**, 3, 4; B. K. I. Meijers, B. Bammens, K. Verbeke, P. Evenepoel, American Journal of Kidney Diseases 2008, 51, 839; L. Philbert, W. Xiaoyang, Current pharmaceutical design **2015**, 21, 1862.

[13]   M. V. Cespedes, U. Unzueta, A. Avino, A. Gallardo, P. Alamo, R. Sala, A. Sanchez-Chardi, I. Casanova, M. A. Mangues, A. Lopez-Pousa, R. Eritja, A. Villaverde, E. Vazquez, R. Mangues, EMBO molecular medicine **2018**, 10.

[14]   F. L. Gordillo Altamirano, J. J. Barr, Clinical microbiology reviews **2019**, 32; S. Hesse, S. Adhya, Annual review of microbiology **2019**, 73, 155.

[15]   O. Krut, I. Bekeredjian-Ding, Journal of immunology **2018**, 200, 3037; C. J. Cooper, M. Khan Mirzaei, A. S. Nilsson, Frontiers in microbiology **2016**, 7.

[16]   K. Dabrowska, P. Miernikiewicz, A. Piotrowicz, K. Hodyra, B. Owczarek, D. Lecion, Z. Kazmierczak, A. Letarov, A. Gorski, Journal of virology **2014**, 88, 12551.

[17]   L. L. Furfaro, M. S. Payne, B. J. Chang, Frontiers in cellular and infection microbiology **2018**, 8, 376; G. J., J. P., *How to Achieve a Good Phage Therapy Clinical Trial?*, Springer, **2019**.

[18]   A. Zoued, Y. R. Brunet, E. Durand, M. S. Aschtgen, L. Logger, B. Douzi, L. Journet, C. Cambillau, E. Cascales, Biochimica et biophysica acta **2014**, 1843, 1664.

[19]   S. V. Rajagopala, S. Casjens, P. Uetz, BMC microbiology **2011**, 11, 213.

[20]   S. D. Benson, J. K. Bamford, D. H. Bamford, R. M. Burnett, Acta crystallographica. Section D, Biological crystallography **2002**, 58, 39.

[21]   S. Mantynen, L. R. Sundberg, H. M. Oksanen, M. M. Poranen, Viruses **2019**, 11.

[22]   Y. Lu, Z. Gu, Nature nanotechnology **2017**, 12, 1023.

[23]   J. D. Mougous, M. E. Cuff, S. Raunser, A. Shen, M. Zhou, C. A. Gifford, A. L. Goodman, G. Joachimiak, C. L. Ordonez, S. Lory, T. Walz, A. Joachimiak, J. J. Mekalanos, Science **2006**, 312, 1526.

[24]   J. Wang, K. Liu, R. Xing, X. Yan, Chemical Society reviews **2016**, 45, 5589.

[25]   J. Sánchez, H. López-Laguna, P. Álamo, N. Serna, A. Sánchez-Chardi, V. Nolan, O. Cano-Garrido, I. Casanova, U. Unzueta, E. Vazquez, R. Mangues, A. Villaverde, Advanced

science **2019**; W. Huang, P. Hao, J. Qin, S. Luo, T. Zhang, B. Peng, H. Chen, X. Zan, Acta biomaterialia **2019**, 90, 441; T. Y. Chen, W. J. Cheng, J. C. Horng, H. Y. Hsu, Colloids and surfaces. B, Biointerfaces **2019**, 110644.

[26]   H. Lopez-Laguna, U. Unzueta, O. Conchillo-Sole, A. Sanchez-Chardi, M. Pesarrodona, O. Cano-Garrido, E. Volta, L. Sanchez-Garcia, N. Serna, P. Saccardo, R. Mangues, A. Villaverde, E. Vazquez, Acta biomaterialia **2019**, 83, 257.

[27]   L. Deng, Z. Feng, H. Deng, Y. Jiang, K. Song, Y. Shi, S. Liu, J. Zhang, S. Bai, Z. Qin, A. Dong, ACS applied materials & interfaces **2019**, 11, 31743; G. P. Howard, G. Verma, X. Ke, W. M. Thayer, T. Hamerly, V. K. Baxter, J. E. Lee, R. R. Dinglasan, H.-Q. Mao, Nano Research **2019**, 12, 837; L. Shang, K. Nienhaus, G. U. Nienhaus, J Nanobiotechnology **2014**, 12, 5; N. P. Truong, M. R. Whittaker, C. W. Mak, T. P. Davis, Expert opinion on drug delivery **2015**, 12, 129.

[28]   U. Unzueta, N. Serna, L. Sanchez-Garcia, M. Roldan, A. Sanchez-Chardi, R. Mangues, A. Villaverde, E. Vazquez, Nanotechnology **2017**, 28, 505102.

[29]   J. B. Bailey, R. H. Subramanian, L. A. Churchfield, F. A. Tezcan, Methods in enzymology **2016**, 580, 223.

[30]   A. Chaudhary, R. D. Yadav, J Nanopart Res **2019**, 21; S. Sikder, V. Gote, M. Alshamrani, J. Sicotte, D. Pal, Expert opinion on drug delivery **2019**, 16, 1113; K. A. Cannon, J. M. Ochoa, T. O. Yeates, Current opinion in structural biology **2019**, 55, 77; Y. Li, Y. Wang, G. Huang, J. Gao, Chemical reviews **2018**, 118, 5359; A. Maham, Z. Tang, H. Wu, J. Wang, Y. Lin, Small **2009**, 5, 1706; U. Unzueta, M. V. Cespedes, E. Vazquez, N. Ferrer-Miralles, R. Mangues, A. Villaverde, Trends in biotechnology **2015**, 33, 253.

[31]   Y. Ma, R. J. Nolte, J. J. Cornelissen, Advanced drug delivery reviews **2012**, 64, 811; M. Karimi, H. Mirshekari, S. M. Moosavi Basri, S. Bahrami, M. Moghoofei, M. R. Hamblin, Advanced drug delivery reviews **2016**, 106, 45.

[32]   A. P. M. Guttenplan, L. J. Young, D. Matak-Vinkovic, C. F. Kaminski, T. P. J. Knowles, L. S. Itzhaki, J Nanobiotechnology **2017**, 15, 70; T. O. Yeates, Annual review of biophysics **2017**, 46, 23; T. D. Sutherland, M. G. Huson, T. D. Rapson, Journal of structural biology **2018**, 201, 76; I. W. Hamley, Biomacromolecules **2019**, 20, 1829.

[33]   O. Cano-Garrido, E. Garcia-Fruitos, A. Villaverde, A. Sanchez-Chardi, Biotechnol J **2018**, 13, e1700388.

[34]   J. M. Sanchez, L. Sanchez-Garcia, M. Pesarrodona, N. Serna, A. Sanchez-Chardi, U. Unzueta, R. Mangues, E. Vazquez, A. Villaverde, Biomacromolecules **2018**, 19, 3788.

[35]   R. Mohana-Borges, J. L. Silva, J. Ruiz-Sanz, G. de Prat-Gay, Proceedings of the National Academy of Sciences of the United States of America **1999**, 96, 7888.

[36]   Y. R. Brunet, J. Henin, H. Celia, E. Cascales, EMBO reports **2014**, 15, 315.
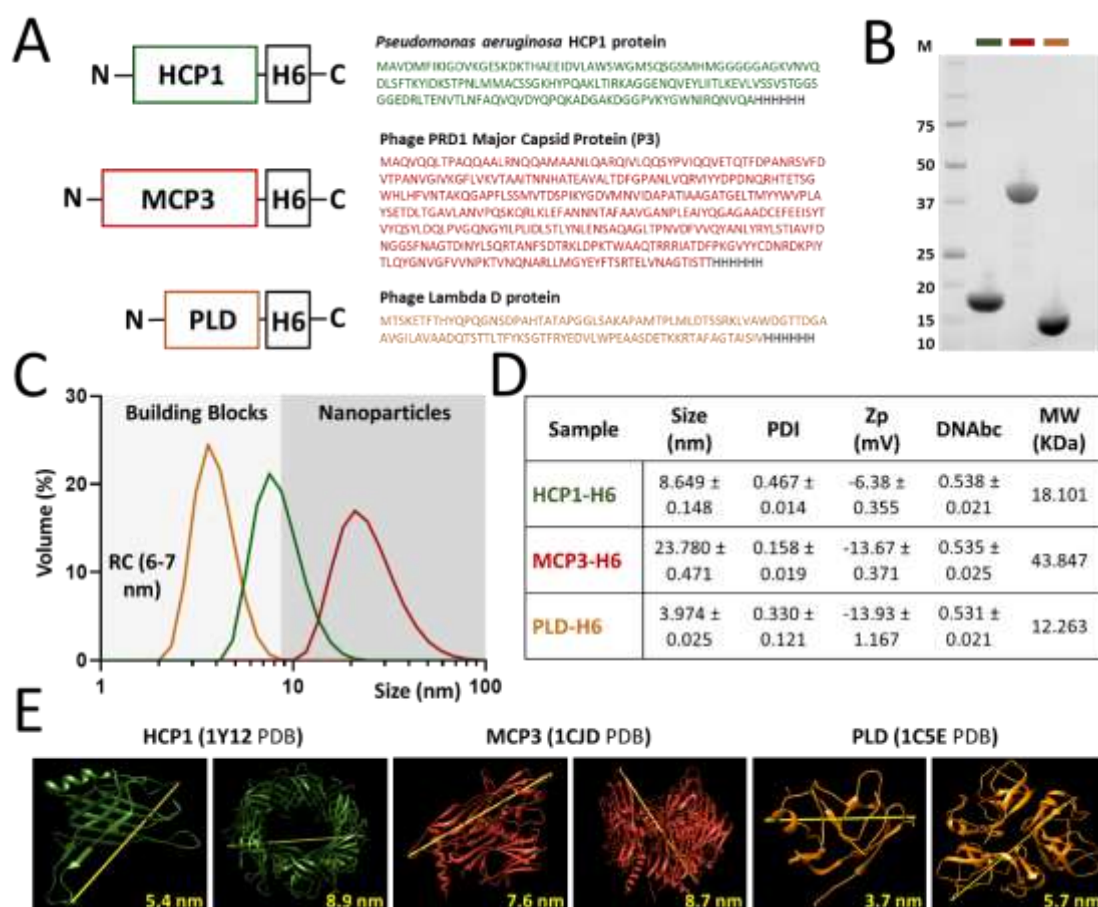
Figure 1. Physicochemical characterization of H6-tagged recombinant proteins. **A.** Modular organization and amino acid sequences of the fusion proteins, from the amino (N) to the carboxy (C) termini. In color we indicate the protein segment from the original source, and in black, the H6 tail. Box sizes are only approximate. **B**. Immunodetection of the constructs through Western Blot (WB) upon affinity purification. M indicates the masses of the molecular weight marker, in KDa. **C**. Size distribution of pure H6-tagged HCP1, MCP3 and PLD proteins in their corresponding buffer is represented as Gaussian plots. The Renal Clearance Threshold or RC (around 8 nm, [22]) is presented in pale grey and nanoparticle (NP) formation over this value, in dark grey. **D**. Relevant physicochemical parameters of purified proteins, namely size in nm and their corresponding Polydispersion Indexes (PDI), surface charge expressed by Zeta potential (Z_p) in mV and bicatenary DNA (DNAbc) content obtained from ratio (A_{260}/A_{280}) (values below 0.57 correspond to nearly 0 % DNA content). The experimental molecular weight (MW) in kDa, obtained from MALDI-TOF assays, is also indicated. **E**. The monomeric as well as the trimeric or hexameric respective structures of all proteins are depicted as deposited in RCSB. MCP3 (pdb 1CJD) and PLD (pdb 1C5E) are naturally trimeric, while HCP1 (pdb 1Y12) forms hexamers [36]. Yellow lines and numbers indicate the maximum diameter of these proteins and complexes.
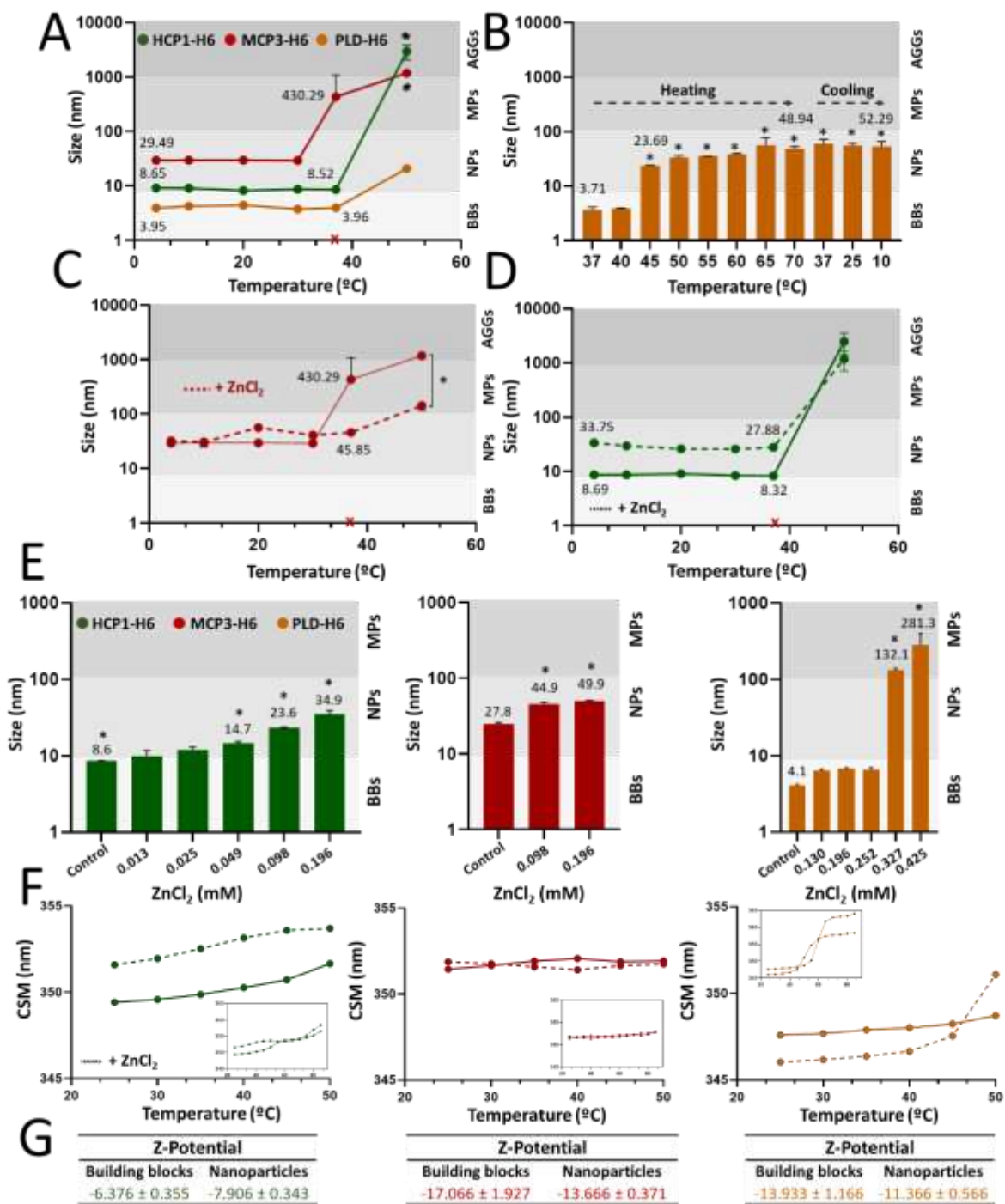
Figure 2. Protein rearrangements into oligomerized nanoscale forms. A. Size analysis of protein constructs HCP1-H6 (in green), MCP3-H6 (in red) and PLD-H6 (in orange) under increasing temperature (from 4 to 50 °C). **B**. Size analysis of PLD-H6 after initial heating (from 37 to 70 °C) and subsequent cooling (from 70 to 10 °C), expressed in both cases with discontinuous arrows. **C**. Size analysis of MCP3-H6 under increasing temperature (from 4 to 50 °C) in p/a of 0.2 mM of $ZnCl_2$. The red x in panels A and C refers to 37 °C, as a reference to the body temperature (BT). **D**. Size analysis of HCP1-H6 under increasing temperature (from 4 to 50 °C) in p/a of 0.2 mM of $ZnCl_2$. **E.** Size analysis of recombinant proteins after increasing concentrations of $ZnCl_2$ (from 0.013 to 0.425 mM) at room temperature (25 °C). **F**.

Centre of Spectral Mass (CSM) study under increasing temperature (from 25 to 50 ℃) in p/a of 0.2 mM of $ZnCl_2$. Small panels correspond to the same analysis under an extended temperature range (from 25 to 87 ℃). **G**. Z-potential determination comparing the monomeric and nanoparticulated proteins forms. Plots are arranged in four different strata according to the material size range. Pale grey corresponds to *Building Blocks* (BBs), semi-pale grey to *Nanoparticles* (NPs), semi-strong grey to *Microparticles* (MPs) and strong grey to *Aggregates* (AGGs). Data are expressed as $\bar{x} \pm$ SEM, n = 3 and the statistical comparison in relation to the starting size (*$p < 0.05$).
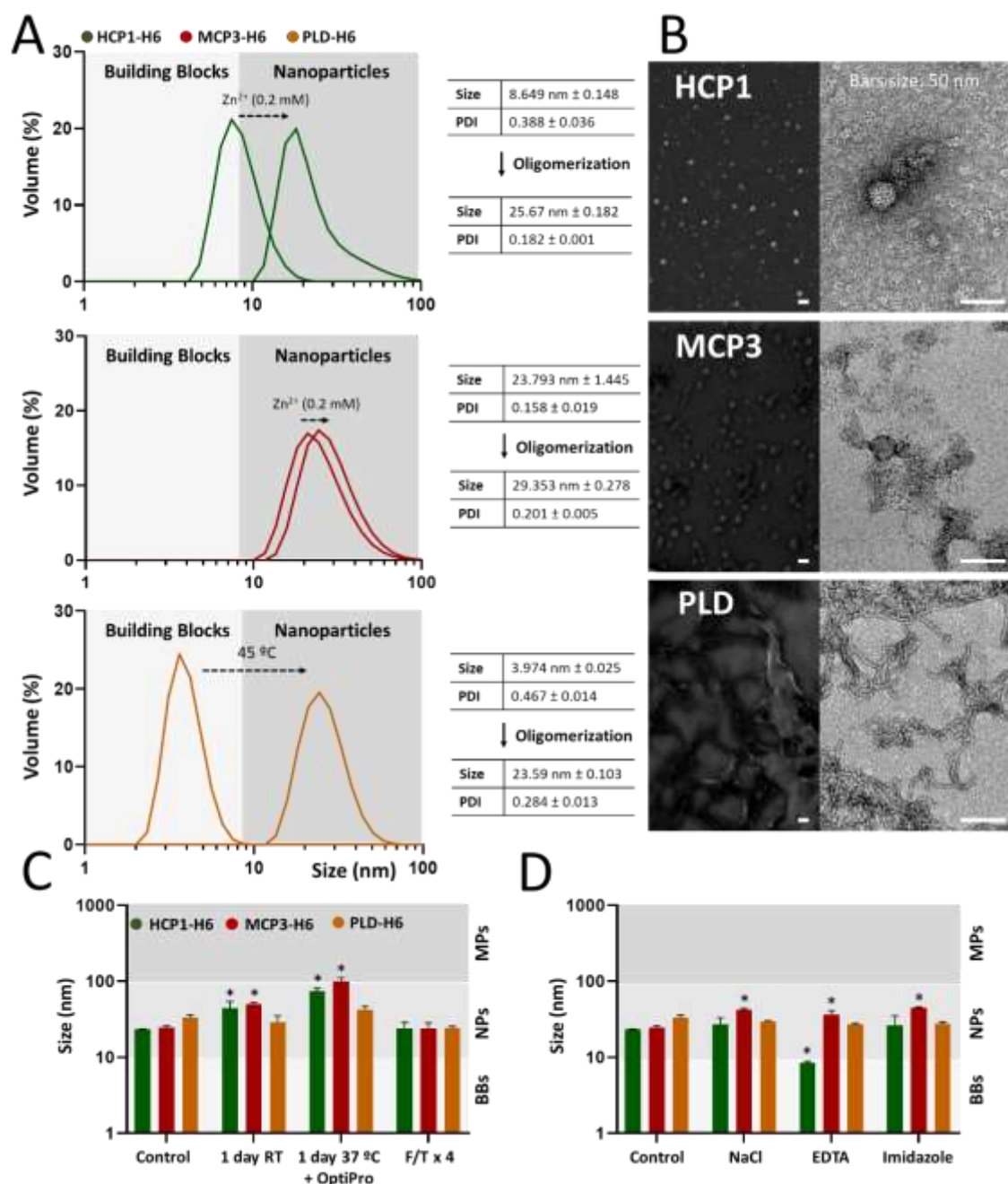
Figure 3. Oligomerization conditions and stability of nanoparticles. A. Size analysis of recombinant proteins after ZnCl$_2$ addition or temperature application. Size and PDI data are expressed in right panels. **B**. Visualization of previous oligomeric structures through FESEM (left) and TEM (right). **C.** Size analysis of all three oligomers in different temperature and complex cell medium conditions. RT corresponds to room temperature and F/T to freezing and thawing. **D**. The same size analysis of panel A but in presence of different chemical compounds such as salt (333 mM), EDTA and imidazole at 0.2 mM. Plots are arranged in two different strata according to the material size range. Pale grey corresponds to *Building Blocks* (BBs) and strong grey to *Nanoparticles* (NPs). Data expressed as $\bar{x}$ ± SEM, n = 3 for panel A.

Data expressed as $\bar{x} \pm$ SEM, n = 3 and statistical comparison in relation to the control group for panels C and D (*p < 0.05).

The human microbiome is a source of structural proteins useful as protein materials for clinical uses by exploiting their self-assembling tendencies and the limited interactivity with human molecules. Two phage and one bacterial proteins are used to explore this concept, through the controlled formation of regular protein nanoparticles, stable under physiological conditions and suitable for further functionalization.

Hèctor López-Laguna, Laura Sánchez-García, Naroa Serna, Eric Voltà-Durán, Julieta M. Sánchez, Alejandro Sánchez-Chardi, Ugutz Unzueta*, Marcin Los, Antonio Villaverde* and Esther Vázquez

Engineering protein nanoparticles out from components of the human microbiome